Wave energy in the Balearic Sea. Evolution from a 29 year spectral wave hindcast

S. Ponce de León[a], A. Orfila[b,*], G. Simarro[c]

[a] UCD School of Mathematical Sciences. Dublin 4, Ireland
[b] IMEDEA (CSIC-UIB). 07190 Esporles, Spain.
[c] Institut de Ciéncies del Mar (CSIC). 08003 Barcelona, Spain.

Abstract

This work studies the wave energy availability in the Western Mediterranean Sea using wave simulation from January 1983 to December 2011. The model implemented is the WAM, forced by the ECMWF ERA-Interim wind fields. The Advanced Scatterometer (ASCAT) data from MetOp satellite and the TOPEX-Poseidon altimetry data are used to assess the quality of the wind fields and WAM results respectively. Results from the hindcast are the starting point to analyse the potentiality of obtaining wave energy around the Balearic Islands Archipelago. The comparison of the 29 year hindcast against wave buoys located in Western, Central and Eastern basins shows a high correlation between the hindcasted and the measured significant wave height (H_s), indicating a proper representation of spatial and temporal variability of H_s. It is found that the energy flux at the Balearic coasts range from 9.1 kW/m, in the north of Menorca Island, to 2.5 kW/m in the vicinity of the Bay of Palma. The energy flux is around 5 and 6 times lower in summer as compared to winter.

Keywords: Mediterranean Sea, WAM model, wave energy, wave climate variability, ASCAT, TOPEX-Poseidon

*Corresponding author
Email address: aorfila@imedea.uib-csic.es (A. Orfila)

1. Introduction

Energy obtained from marine devices is one of the most promising renewable energy resources in coastal areas as the technology in wave energy converters (WEC hereinafter) is becoming more efficient (Waters et al., 2009; Iglesias and Carballo, 2010a,b). To properly characterize the potential of the wave energy in a specific area, it is crucial to have an accurate analysis of the wave climate so as to dimension the WECs maximizing the energy obtained from the waves.

In the Balearic Sea, the most western basin of the Mediterranean Sea, the wave climate has already been identified to have, in general, a complex pattern as the result of the variability in the storm tracks, the complex orography and the relatively short fetch (Canellas et al., 1997; Ponce de León and Orfila, 2013). Due to the complexity in the wave pattern, the search for appropriate locations for WECs has to account both for those locations where maximum energy is found but also maintained during large periods (Parkinson et al. , 2015).

In the last decade the wave forecast has improved significantly, thanks to 1) the advance in the numerical models used for wave forecasting (in terms of physical processes resolved as well as in the numerical algorithms implemented), 2) the increase in the number of wave measurements (moorings, radar from satellite or coastal stations) and 3) the advances in data assimilation techniques. Today it is possible to compile large databases of wave parameters that are routinely used for prognostic or diagnostic purposes (Ratsimandresy et al. , 2008; Appendini et al., 2015).

Numerical studies for wave power considerations are mostly performed in areas with a high potential in wave energy generation. Since wave power is directly related with the significant wave height, H_s, and the energy period, T_e, coastal seas with moderate wave climate, such as the Mediterranean Sea, have not been fully studied. The above in spite that, under a technical and economical perspective, areas with moderate but sustained wave climate are very appropriate for the installation of power farms where the WECs will be able to operate during larger periods (Liberti et al., 2013).

Wave conditions are certainly the major factor affecting wave energy production and a significant part of the energy will be obtained from exceptional wave conditions during extreme events. However, such conditions pose serious engineering challenges and increase the costs in the development of the WECs and therefore intricate the energy production, device installation and maintenance as well as the transport of energy. On the other hand, in calmer and semi-enclosed seas with relative moderate wave conditions such as the Mediterranean sea, many technical issues related to extreme sea climate could be more easily solved, possibly making wave energy production economically viable.

The Balearic Archipelago (Northwestern Mediterranean Sea) is formed by four major islands (Mallorca, Menorca, Ibiza and Formentera). It is one of the largest touristic spots around the globe, hosting in 2014 more than 14 millions tourists and having a permanent population of 1.2 millions (80% of the population in Mallorca). The floating population oscillates seasonally from 2.6 millions during August to 140.000 in December, demanding goods and services that have to be imported from mainland (including energy).

Following these antecedents, this work studies the wave energy assessment in the Balearic Islands using a new wind-wave data base covering from 1983 to 2011. The paper first presents the new wave database generated by the WAM 4.5.2 model (Günther and Berehns, 2011), while wind is given by the ECMWF ERA-Interim reanalysis (Dee et al., 2011) retrieved at a horizontal resolution of 0.125° (14 km). Next, wave climate is characterized by means of an EOF analysis of the significant wave height. Finally, a wave power analysis is presented for coastal stations around the Balearic Islands located at intermediate depths.

2. Data and Methods

2.1. Wave model set-up

The wave model implemented is the third generation spectral wave model WAM (Komen et al., 1994). A high resolution grid was implemented covering the whole Mediterranean Sea, extending from 30° N to 46° N and 06° W to 37° E. All the spectral components are calculated prognostically from the energy-balance equation up to a variable cut-off frequency (WAMDI group , 1988).

A 29 years hindcast, from January 1983 to December 2011, was performed for the entire Mediterranean Sea using ECMWF ERA-Interim wind fields (`http://www.ecmwf.int`). Numerical parameters of the present WAM configuration are summarized in Table 1. WAM model input/output time step was set as 6 hours since finer resolution does not add detail to the subject of this work. The wind fields retrieved were interpolated into the wave model computational grid.

2.2. Wave and wind observations

Several sources from different buoy networks have been used for the validation of the wave hindcast. These data sets are distributed by the JCOMM Project (Bidlot, 2012). The first set of buoys belong to the Spanish network and are operated by the Spanish Harbor Authority (Puertos del

Estado). The buoys considered are 1) the Cabo Begur buoy at 41.92° N, 03.65° E moored at 1200 m depth; 2) the Dragonera buoy, at 39.56° N, 02.10° E, moored at 135 m and 3) the Buoy of Maó at 39.72°N, 04.42° E which is moored at 300 m (see Figure 1,a points B1, B2 and B3 respectively). The buoys measure met-ocean variables and are wave scan directional.

For the Ionian Sea we use the Crotone buoy (B4 in Figure 1,a) from the Rete Ondametrica Nazionale (RON), located at 39.01° N, 17.31° E, which is moored at 615 m (Corsini et al., 2004; Vicinanza et al., 2011).

In the east side the Greek POSEIDON network formed by Seawatch buoys are used (Mazarakis et al., 2012). Here we use data from Athos and Santorini buoys located in the Aegean Sea (B5 and B6, respectively in Figure 1,a)) because registers from these buoys had a long coverage of more than 11 years since year 2000, coincident with the study period. Santorini is located South-East of Santorini Island in 36.20° N, 25.50° E and is moored at 280 m. Athos is located South of Athos peninsula in 39.96° N, 24.72° E and is moored at 220 m.

For the verification of the ECMWF ERA-Interim wind fields, we use the MetOP-A ASCAT Level 2 product, consisting in the wind at 10 m above the ocean surface. This product has a spatial resolution of 12.5 km.

The altimeter from TOPEX-Poseidon was launched on August 10^{th} 1992 to map the ocean surface topography and operates at two frequencies: 13.6 GHz in the $\mathrm{Ku-band}$ and 5.3 GHz in the $\mathrm{C-band}$. Here, the assessment of wave hindcast is made by the use of $\mathrm{H_s}$ measured by TOPEX-Poseidon/Jason-1 included in the GLOBWAVE data base (Ash et al., 2012). The TOPEX-Poseidon calibrations are taken from Queffeulou and Croize-Fillon (2012).

3. Wave field and wave hindcast validation

3.1. ECMWF ERA-Interim against ASCAT

The 6 hours ECMWF ERA-Interim data-set was compiled for the period between 1983-2011. ASCAT wind data were not used by ERA-Interim and here we have not performed any correction for ERA-Interim. In the Mediterranean, the accuracy of the winds is crucial for wave modeling. Cavaleri and Sclavo (2006) treated this issue pointing out that in coastal areas, the model winds are unreliable because of the dominant influence of the orography that is not properly represented in the meteorological model because of its limited resolution. For validation purposes, this data set is compared against the measurements from ASCAT Met-Op over the entire Mediterranean Sea for the period between October 1^{st} and October 15^{th} 2010. The number and coverage of ASCAT observations are sufficiently dense over the whole basin (234.261 observations for this period) for validation purposes (see Figure 2,a for the distribution of measurements).

Comparison of both data sets reveal a good agreement between ECMWF winds and the ASCAT measurements, with a correlation coefficient r = 0.90, slope s = 0.91 and a scatter index (SI) defined as the standard deviation of the predicted data with respect the best-fit line, divided by the mean observations of SI = 0.22 (Figure 2,b).

3.2. WAM model results against TOPEX-Poseidon data

The hindcast is validated against H_s derived from TOPEX-Poseidon altimeter for November 2001 following Caires and Sterl (2003). Satellite tracks for this period are depicted in Figure 3,a. H_s inferred from the along tracks of TOPEX-Poseidon are plotted against wave model hindcast extracted at the same time and location of the satellite measurement in Figure 3,b. Statistics for this comparison show good agreement in the whole basin with a low scatter index of SI = 0.17 with high correlation (r = 0.95).

3.3. WAM wave model results against wave buoy

Finally, wave hindcast is validated with the measurement from the Spanish, the Italian and the Greek buoys networks. As mentioned, six buoys distributed along the Eastern, Central and Western basins, chosen with a sufficient long record, were selected for the validation (white circles in Figure 1,a).

Statistical analysis shows good correlation between the hindcasted and measured significant wave height H_s at the Cabo Begur buoy (B1 in Figure 1) for the 10-year period analyzed. Scatter plot for the buoy and modeled H_s reveals again very good agreement with r = 0.93 and SI = 0.27 (Figure 4, left panel).

In the Balearic Islands Archipelago, the validation of the hindcast is performed against Dragonera Buoy (B2 in Figure 1,a) for the period from November 2006 to November 2011. The scatter plot (Figure 4, right panel) reveals also a good adjustment of the modeled data, with a linear correlation of r = 0.93 and a scatter index of SI = 0.23.

For all the buoys, the agreement between model hindcast and buoys are summarized in Table 2.

4. Wave height variability in the Mediterranean Basin

Time average of H_s shows that the larger values are located in the north-western basin and at the eastern part of the Island of Crete, two areas with strong local winds. The Gulf of Lions is greatly influenced by the Pyrenees to the west and by the Alps to the east, being two decisive boundaries that drive locally intense wind over the Ligurian Sea (Orfila et al., 2005). The combination of wind intensity and wind direction acting over a large area (fetch) generates strong sea states as depicted in Figure 5 (top panel). The larger values of H_s extend from the Gulf of Lions to the southwestern side of Corsica through the Balearic Sea, with an average value of $H_s \sim 1.2$ m for the considered period. Besides, there is a seasonal behaviour of the wave climate with maximum records occurring from December to February (average values of $H_s > 1.1$ m and minimum values between June and August (average values of $H_s < 0.6$ m), as shown in Figure 5 (bottom panel).

Similarly, to the east, in the Aegean Sea, the prevailing winds during summer are the result of the deep continental depression centred over the Northwest of India. These winds that are known either as Meltemi or Etesians by the Turks and Greeks respectively, blow over the Aegean Sea reaching the Island of Crete where intense wave events are recorded.

In order to elucidate in more detail the spatio-temporal distribution of the wave climate in the whole basin, the monthly averaged H_s fields are decomposed using an Empirical Orthogonal Function (EOF) analysis (Emery and Thomson, 2004). The main part of the variability in the H_s fields can be explained using the first three EOFs modes which account for the 85% of the time-wise variance of the wave field.

The first three EOF's (which explain 71.8%, 9.5% and 4% of the variance respectively) are shown in Figure 6 (left panel for the spatial models and central panels for their corresponding amplitudes). The first EOF is the modulation of the mean field as an intensification or weakening of H_s through the annual oscillation of its amplitude (Figure 6, top central panel). The FFT of this amplitude reveals that the main part of the energy contained in the amplitude of the first mode is concentrated at a frequency of $0.0027\,\mathrm{days}^{-1}$ (*i.e.* a period of 1 year) and some of the energy at larger frequencies, $0.0082\,\mathrm{days}^{-1}$ (approximately 4 months).

The second EOF displays an oscillating pattern with positive/negative values of $\mathrm{H_s}$ in the western part and coincident negative/positive values in the eastern basin (Figure 6 middle, left for the mode and central panel for the amplitude). This spatial pattern is indicative of the influence in the wave climate of specific modes of oscillations of the Mediterranean basin such as the Mediterranean Oscillation Index (Gomis et al., 2008). Spectral analysis of the second amplitude reveals that the main pattern of variability is found at a frequency of $0.0055\,\mathrm{days}^{-1}$ (periods of 6 months) (Figure 6, right).

The third EOF shows positive/negative anomalies in the Balearic Sea and in the Aegean Sea with simultaneous negative/positive anomalies at the southern side of Sicily extending up to the Libyan coasts. The amplitude of this mode shows the main energy at the annual period but some energy also at a semi-annual period (Figure 6, bottom panels, left central and right panels for the mode, amplitude and spectra respectively).

As explained below, wave energy flux is dependent on the wave height and the variability on the specific EOF modes provide an additional explanation for the spatio-temporal variability on the available energy in the basin.

5. Wave energy assessment in the Balearic Islands

A set of 9 virtual buoys surrounding the coasts of the three major Balearic Islands (Mallorca, Menorca and Ibiza) are selected in order to assess the potential for wave energy. These buoys are the hindcast presented in the previous section and are selected to be in deep waters in order to have an accurate representation of the wave field given by the numerical model (Figure 1, lower panel). Location and depth of the buoys is indicated in Table 3.

The variation of wave energy is computed following (Waters et al., 2009) as:

$$J = \frac{\rho g^2}{64\pi} \mathrm{T_e} \mathrm{H_s}^2, \tag{1}$$

where J is the energy flux (units of Watts per meter of wave crest), ρ the sea water density (*i.e.* 1027kg/m^3), g the acceleration of gravity, $\mathrm{T_e}$ (or T_{m-10}) the energy period and $\mathrm{H_s}$ the significant wave height. The energy period for a sea state given by a directional wave energy density spectrum F is defined as,

$$T_e = \frac{\displaystyle\int_0^{2\pi}\int_0^{\infty} \sigma^{-1} F \; d\sigma d\theta}{\displaystyle\int_0^{2\pi}\int_0^{\infty} F \; d\sigma d\theta}. \tag{2}$$

The spatial distribution of the temporal mean of the wave power is shown in Figure 7 for the period of 1983-2011. Averaged values of wave power over 15 kW/m are obtained in the central part of the sub basin and the minimum values at the lee of the Islands. Regarding the Balearic Islands, the maximum values in wave power are in the north part of Menorca Island, which is well oriented to the northern fetch, but some other locations such as the north and east side of the island of Mallorca could also have the potential for the installation of WEC. This average is the result of the combination of all sea states which are the combination of pairs of wave height and wave period with a large variability.

Mean and maximum energy flux for the selected locations are depicted in Table 3 and show that they differ in one or two orders of magnitude. The average energy flux presents a large spatial variability with the lowest values located at the vicinity of the Bay of Palma (gauge 6 in Figure 8) with a mean value of $2.5 \pm 0.3\,\mathrm{kW/m}$ whereas the maximum energy flux is obtained at the northern side of Menorca Island (gauges 8 and 9 in Figure 8) with mean values in the energy flux of $8.9 \pm 2.4\,\mathrm{kW/m}$ and $9.1 \pm 2.5\,\mathrm{kW/m}$ respectively.

For design purposes, it is important to have a proper dimension of the WECs for the most common wave power (the most probable combination of $\mathrm{H_s}$ and $\mathrm{T_e}$) rather than the mean or maximum wave power. This analysis is performed by representing the yearly distribution of the averaged energy in terms of $\mathrm{H_s}$ and $\mathrm{T_e}$. For the selected locations surrounding the Balearic Islands the scatter plot of the wave energy is displayed in Figure 8. The color in the plot represents the yearly average distribution of energy in $\mathrm{kWh/(m \cdot year)}$ where the contribution to the total energy given by each sea state is computed by grouping the 6 hours model output in bins of $\mathrm{H_s} = 0.25\,\mathrm{m}$ and $\mathrm{T_e} = 0.25\,\mathrm{s}$ and wave power is computed using Eq. (1). In each of these plots, we indicate the location of the virtual buoy used for the analysis by a star in the map as well as the wave rose at the node in the upper right side. As already indicated, the availability of energy is higher at the two locations at the North of Menorca (nodes 8 and 9) where the annual wave power is concentrated in waves with large wave heights ($\mathrm{H_s} > 2\,\mathrm{m}$) and wave periods ($\mathrm{T_p} > 8\,\mathrm{s}$). At node 2 (located at the west side of the Island of Mallorca), the scatter diagram for the annual energy transport shows a bimodal distribution where the wave power can be obtained by the combination of relatively small wave heights with large periods but also by waves with larger H_s resulting from specific storms. In the graphics, dashed lines correspond to contour lines of constant wave power.

The variability in the wave energy flux has, also, a markedly seasonal distribution as expected from the EOF analysis. The average energy flux on a monthly basis is shown in Figure 9 together with the standard deviation for the whole period under consideration. As a general trend, the wave flux has the maximum values during the end of autumn and during winter, decreasing during spring and with its minimum value between June and August that is roughly $5-6$ times smaller than the winter value. For energy conversion purposes it is convenient to estimate the interannual variability in the wave power. This can be done by using the Coefficient Of Variation (COV) which is defined as the ratio between the average and the standard deviation of the mean wave power flux. The COV measures the deviation from the average value and provides a measure of the temporal variability of wave power (Liberti et al., 2013). The larger values of COV (Figure 9) are found at the locations with higher energy (those oriented to the north (*i.e.* nodes 1, 7, 8 and 9 in Figure 8). At node 2, the value of COV = 0.25 is the result of the bimodal distribution in the scatter diagram observed in Figure 8.

Percentage of non-exceedance of monthly energy flux provided by all sea states are given in Figure 10. For the sake of clarity we represented only the upper 50% of the distribution and the color-bar has been bounded to be 5 times the value of the annual mean of the energy flux (see Table 3). For all the locations, from November to February, 15% of the time the energy flux is 5 times larger than the annual mean. Conversely, during the summer season only the 2% of the time the energy flux reaches this value. Again, the larger seasonal variations are found at the nodes located at the north part of the

Archipelago and the smaller at the lee of the Islands (South). For node #9, during winter, the 70% exceedance is 9.5 kWh/m and the 90 % exceedance is 45.4 kWh/m, while during summer the 70% exceedance is 1.9 kWh/m and the 90 % exceedance 8.3 kWh/m. By contrast, at location #6, during winter the 70% exceedance is 2.4 kWh/m and the 90 % exceedance is 8.9 kWh/m, while in summer the 70% exceedance is 0.7 kWh/m and the 90 % exceedance 1.5 kWh/m. Finally, it is of mention that in order to properly assess the potential of WEC it is convenient to simulate the power output generated by the converters that can be achieved by using the power conversion matrix recently available (Reikard , 2013).

6. Conclusions

Wave climate for the Balearic Island Archipelago has been analysed by performing a 29 year hindcast of the wave field. The numerical simulation has been performed for the entire Mediterranean Sea, and validated using buoys data. The 6 hours wave climate has been used to infer the energy flux in shallow areas of the Archipelago. The energy flux has been found to present a large spatial and temporal variability with mean values ranging from 9.1±2.5 kW/m at the north of the Island of Menorca to 2.5±0.3 kW/m at node 6 located in the vicinity of the Bay of Palma. Locations at the north of Menorca oriented to the main fetch are those with the largest values in the energy flux, diminishing in the southern Islands due to the sheltering effect and the change in the incoming wave direction. The energy flux shows a large seasonal variation, being 6 times larger during the winter than during the summer. For the design of the WEC it has to be taken into account that the energy flux gives values that are between 5 times and an order of magnitude larger in winter than in summer for the 90% of exceedance which has to be taken into consideration for failure prevention.

7. Acknowledgments

AO thanks financial support from the ENAP-Colombian Army. GS is supported from the Spanish government through the Ramon y Cajal program.

8. References

Appendini, C. M., Urbano-Latorre, C. P., Figueroa, B., Dagua-Paz, C. J., Torres-Freyermuth, A., Salles, P., 2015. Wave energy potential assessment in the caribbean low level jet using wave hindcast information. Applied Energy 137 (0), 375 – 384.

Ash, E., Busswell, G., Pinnock, S., 2012. DUE GlobWave Wave Data Handbook. Logica, UK.

Bidlot, J., November 2012. Intercomparison of operational wave forecasting systems against buoys: data from ecmwf, metoffice, fnmoc, msc, ncep, meteofrance, dwd, bom, shom, jma, kma, puerto del estado, dmi, cnr-am, metno, shn-sm. Tech. rep., European Centre for Medium-range Weather Forecasts.

Caires S, Sterl A., 2003. Validation of ocean wind and wave data using triple collocation. Journal of Geophysical Research 108 (3098),16.

Canellas, B., Orfila, A., Méndez, F., Menéndez, M., Tintoré, J., 1997. Application of a pot model to estimate the extreme significant wave height levels around the balearic sea (western mediterranean). Journal of Coastal Research 50, 329–333.

Cavaleri, L., Sclavo, M., 2006. The calibration of wind and wave model data in the Mediterranean Sea. Coastal Engineering 53 (7), 613–627.

Corsini, S., Franco, L., Piscopia, R., Inghilesi, R., 2004. Latlante delle onde nei mari italiani-italian wave atlas. tech. rep., apat. Tech. rep., ISPARA.

Dee, D. P. and Uppala, S. M., Simmons, A. J., Berrisford, P., Poli, P., Kobayashi, S., Andrae, U., Balmaseda, M. A., Balsamo, G., Bauer, P., Bechtold, P., Beljaars, A. C. M., van de Berg, L., Bidlot, J., Bormann, N., Delsol, C., Dragani, R., Fuentes, M., Geer, A. J., Haimberger, L., Healy, S. B., Hersbach, H., Hlm, E. V., Isaksen, L., Kllberg, P., Khler, M., Matricardi, M., McNally, A. P., Monge-Sanz, B. M., Morcrette, J.-J., Park, B.-K., Peubey, C., de Rosnay, P., Tavolato, C., Thpaut, J.-N., Vitart, F., 2011. The ERA-Interim reanalysis: configuration and performance of the data assimilation system. Quarterly Journal of the Royal Meteorological Society 137 (656), 553–597.

Emery, W.-J., Thomson, R.-E., 2004. Data Analysis Methods in Physical Oceanography. Elsevier H.V., Netherlands.

Gomis, D., Ruiz, S., Sotillo, M. G., Alvarez-Fanjul, E., Terradas, J., 2008. Low frequency mediterranean sea level variability: The contribution of atmospheric pressure and wind. Global and Planetary Change 63 (23), 215–229.

Günther, H., Berehns, A., 2011. The WAM model validation document version 4.5.2. Institute of Coastal Research Helmholtz-Zentrum Geesthacht, Germany.

Hasselmann, S. K., Hasselmann, J., Allender, H., Barnett, T. P., 1985. Computations and parameterizations of the nonlinear transfer in a gravity-wave spectrum. part ii. parameterizations of the nonlinear transfer for application in wave models. Journal of Physical Oceanography 15, 1378 – 1391.

Hodur, R. M., 1997. The naval research laboratorys coupled ocean/atmospheric mesoscale prediction system (coamps). Monthly Weather Review 125, 1414–1430.

Iglesias, G., Carballo, R., 2010a. Offshore and inshore wave energy assessment: Asturias (n spain). Energy 35 (5), 1964 – 1972.

Iglesias, G., Carballo, R., 2010b. Wave energy resource in the estaca de bares area (spain). Renewable Energy 35 (7), 1574 – 1584.

Komen, G. J., Cavaleri, L., Donelan, M., Hasselmann, K., Hasselmann, S., Janssen, P. A. E. M., 1994. Dynamics and Modelling of Ocean Waves. Cambridge University Press, UK.

Liberti, L., Carillo, A., Sannino, G., 2013. Wave energy resource assessment in the mediterranean, the italian perspective. Renewable Energy 50 (0), 938 – 949.

Mazarakis, N., Kotroni, V., Lagouverdos, K., Bertotti, L., 2012. High-resolution wave model validation over the Greek maritime areas. Nat. Hazards Earth Syst. Sci. 12, 3433–3440.

Orfila, A., Alvarez, A., Tintore, J., Jordi, A., Basterretxea, G., 2005. Climate teleconnections at monthly time scales in the ligurian sea inferred from satellite data. Progress in Oceanography 66 (24), 157–170.

Ponce de León, S., Orfila, A., 2013. Numerical study of the marine breeze around the Mallorca island. Applied Ocean Research 40, 26–34.

Queffeulou, P., Croize-Fillon, D., 2012. Global altimeter hs data set. Tech. rep., IFREMER.

Parkinson, S. C., Dragoon, K., Reikard, G., Garca-Medina, G., Ozkan-Haller, H.T., Brekken, T.K.A., 2015. Integrating ocean wave energy at large-scales: A study of the US Pacific Northwest. Renewable Energy, 76, 551–559.

Ratsimandresy, A.W., Sotillo, M.G., Carretero-Albiach, J.C., Alvarez-Fanjul, E., Hajji, H., 2008. A 44-year high-resolution ocean and atmospheric hindcast for the Mediterranean Basin developed within the HIPOCAS Project, Coastal Engineering 55,827–842.

Reikard, G., 2013. Integrating wave energy into the power grid: Simulation and forecasting. Ocean Engineering, 73, 168 –178.

Vicinanza, D., Cappietti, L., Ferrante, V., and Contestabile, P., 2011. Estimation of wave energy in the Italian offshore. Journal of Coastal Research SI (64), 613 – 617.

WAMDI group, 1988. The WAM model– a third generation ocean wave prediction model. Journal of Physical Oceanogry 18, 1775 – 1810.

Waters, R., Engström, J., Isberg, J., Leijon, M., 2009. Wave climate off the swedish west coast. Renewable Energy 34 (6), 1600 – 1606.

Parameter	Grid details
Integration time step	120 seconds
Spatial resolution	0.25° (27.8 km)
Number of points (lon,lat)	173 × 65
Propagation	Spherical
Frequencies	30
Directional bands	36
Frequency domain (Hz)	0.04177 - 0.41145
Latitude coverage	30° N - 46° N
Longitude coverage	6° W- 37° E
Wind input time step (hours)	6
WAM output time step (hours)	6
ECMWF spatial resolution	Gaussian linear grid at T255 resolution retrieved at 0.125°

Table 1: Numerical parameters for the Mediterranean Sea WAM model configuration.

	B1	B2	B3	B4	B5	B6
Slope	0.94	0.82	0.88	0.80	0.91	1.08
S.I.	0.27	0.23	0.21	0.24	0.20	0.16
Bias	0.06	0.18	0.12	0.05	0.11	0.09
r	0.93	0.93	0.81	0.79	0.78	0.85

Table 2: Slope, Scatter Index (S.I.), bias and correlation coefficient (cc) between the model and the analyzed buoys.

Gage	Lat	Lon	Depth (m)	$J_{mean} \pm std$ (kW/m)	J_{max} (kW/m)	$\mathrm{H_s}$ (m)	$\mathrm{H_{s,max}}$ (m)
1	3.50°E	40.00 °N	139	5.9 ± 1.8	507.2	0.9	9.1
2	2.50°E	39.83°N	79	3.6 ± 0.9	419.0	0.7	8.5
3	1.17°E	39.17°N	250	3.6 ± 0.6	347.8	0.8	7.8
4	1.50°E	38.50°N	67	3.4 ± 0.3	253.6	0.8	6.6
5	1.67°E	38.83°N	108	3.6 ± 0.4	333.5	0.8	7.7
6	2.67°E	39.17°N	54	2.5± 0.3	193.3	0.7	6.1
7	3.50°E	39.50°N	73	4.8 ± 1.2	329.2	0.9	7.3
8	4.50°E	39.83°N	210	8.9 ± 2.4	577.6	1.1	9.4
9	4.50°E	40.00°N	220	9.1 ± 2.5	583.8	1.1	9.6

Table 3: Coordinates and depth of the virtual buoys analyzed together with mean and maximum energy flux and wave height.

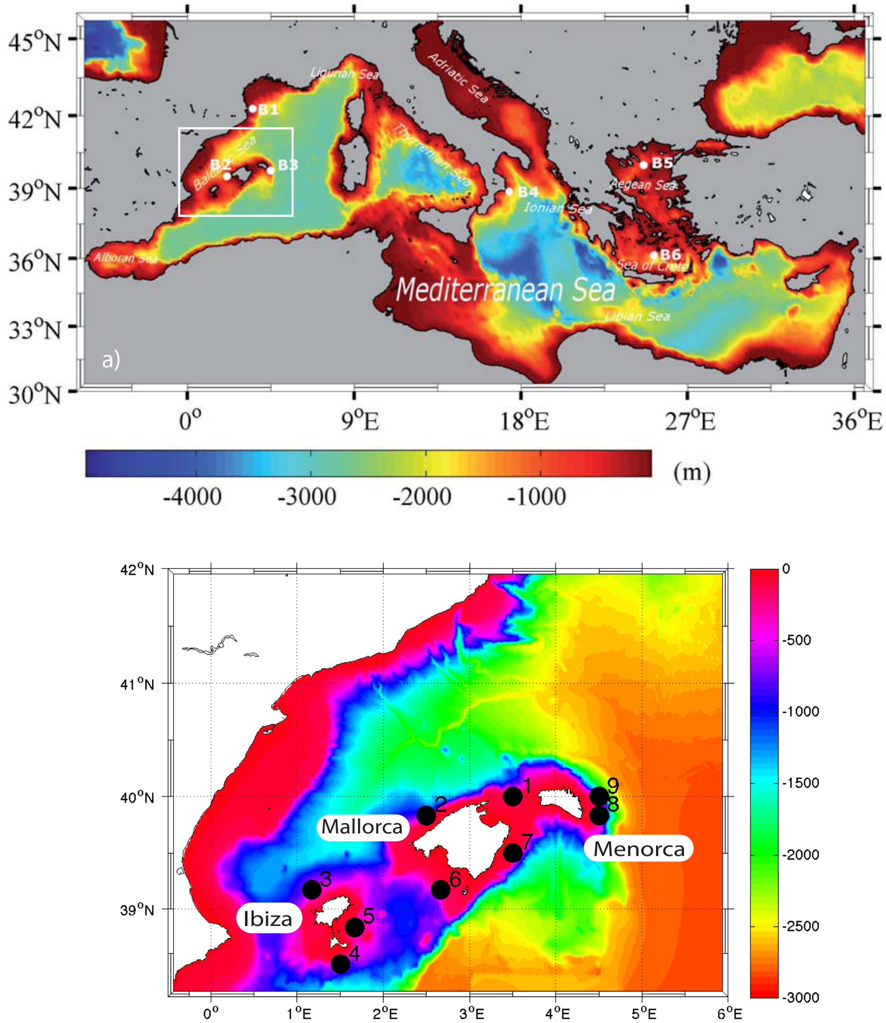

Figure 1: Bathymetry of the Mediterranean Sea and domain of the hindcast. The position of the wave buoys used for the validation are depicted asd B1 for Cabo Begur; B2 for Dragonera; B3 for Maó; B4 for Crotone; B5 for Athos and B6 for Santorini. The location of the virtual buoys around the Balearic Islands used for the energy assesment are shown in the lower panel.

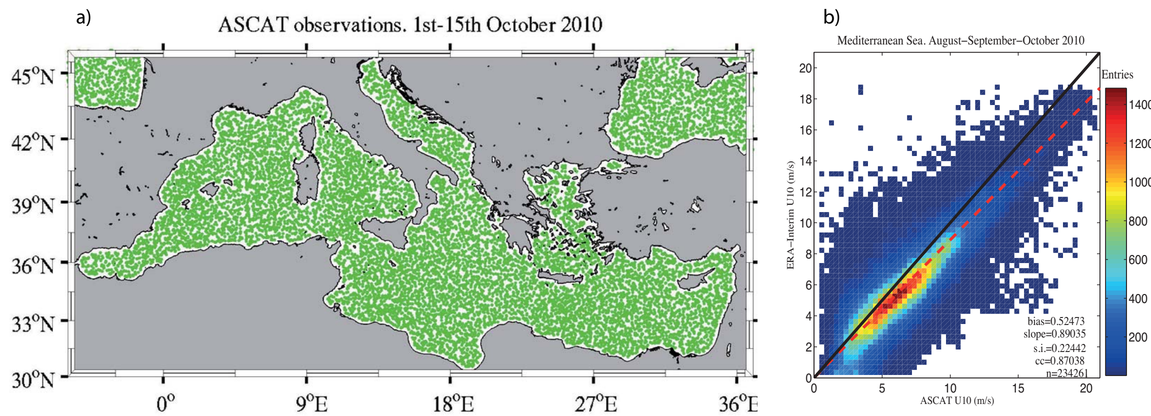

Figure 2: a) ASCAT observations on the Mediterranean Sea during the period of 1st-15th October 2010. (green points denote the locations where the data were measured by MetOp satellite). b) Scatter plot for the wind speed (U_{10}) after the collocation between ASCAT data against the ECMWF ERA-Interim analysis during the first 15 days of October 2010. Colors indicate the number of entries.

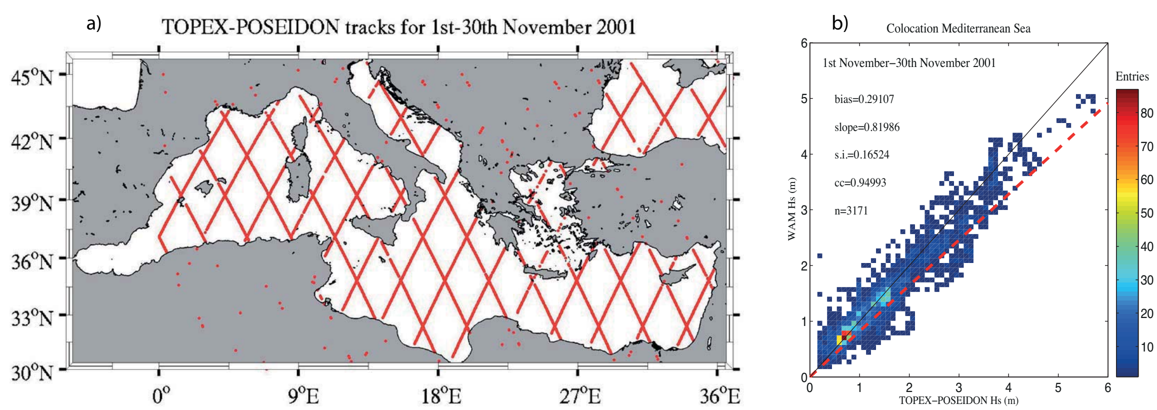

Figure 3: a) TOPEX-POSEIDON tracks during November 2001. b) Scatter plot between sea surface height from TOPEX-POSEIDON and WAM hindcast for November of 2001. Colors indicate the number of entries.

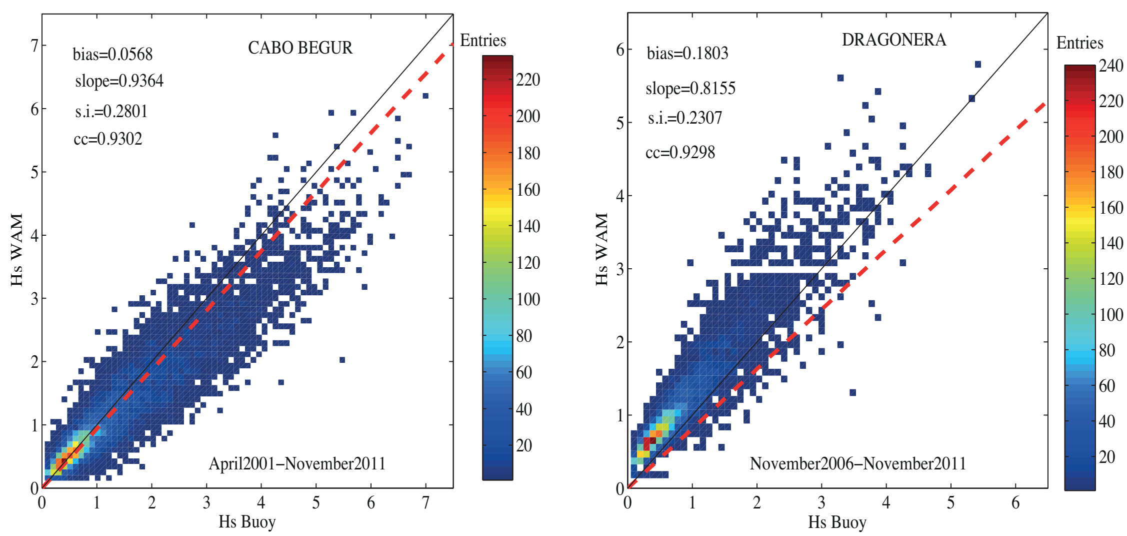

Figure 4: Scatter plots of significant wave height H_s from buoy and model at Cabo Begur (left panel) and Dragonera (right panel). The number of records are $N = 10735$ and $N = 7268$ respectively. Colors indicate the number of entries.

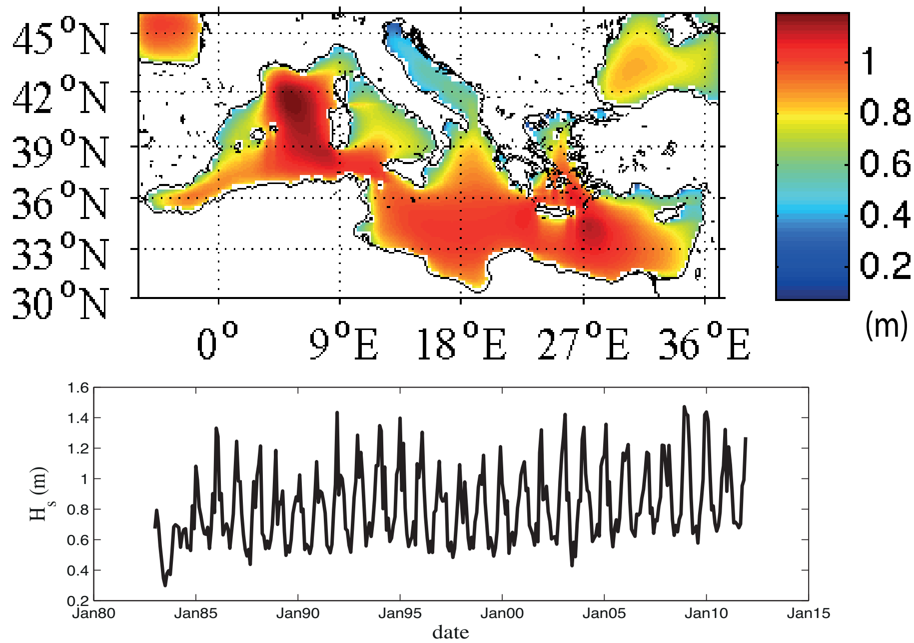

Figure 5: Spatial distribution of H_s averaged for January 1983 to December 2011 (top panel). The temporal evolution of H_s spatial mean for the whole basin is displayed for the same period at the bottom panel.

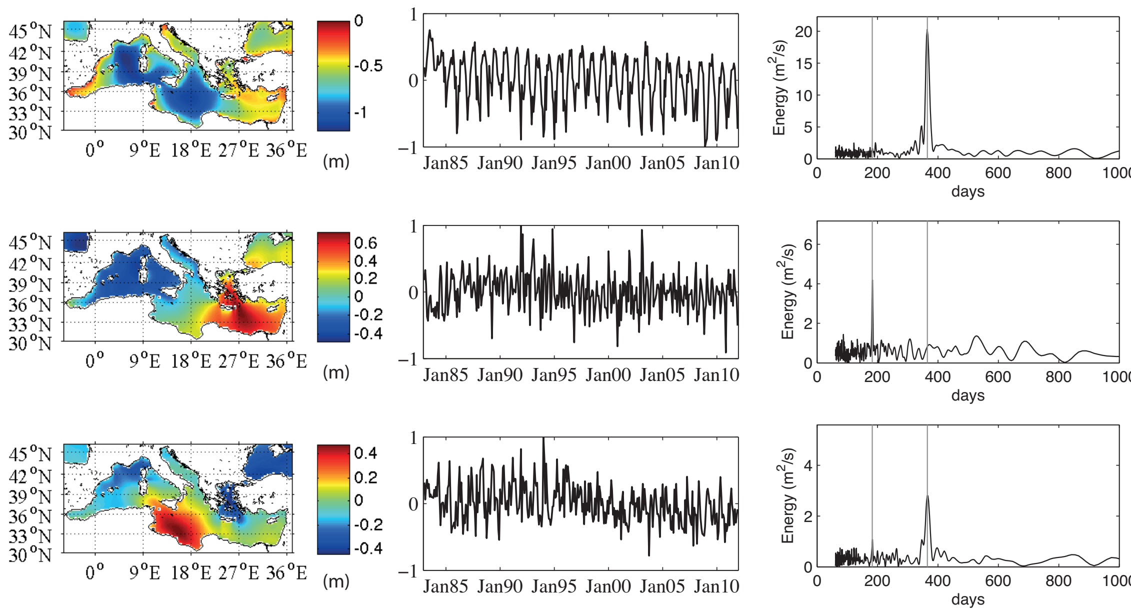

Figure 6: Right panel: spatial pattern of the first (top), second (center) and third EOF (bottom) of the H_s. Units in meters. In the central panel are displayed the corresponding amplitudes and at the right their energy spectra (m^2/s).

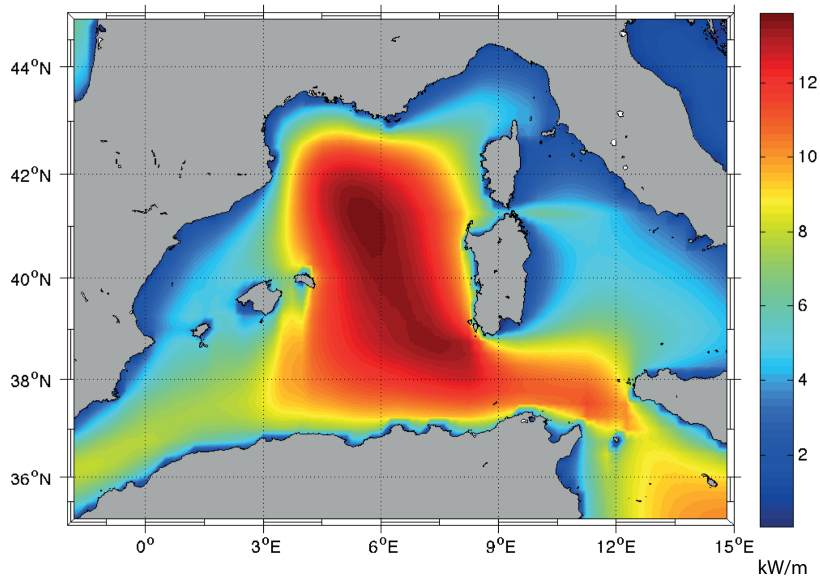

Figure 7: Spatial distribution of the time averaged wave power in kW/m for the period between 1983 and 2011 in the Western Mediterranean Sea.

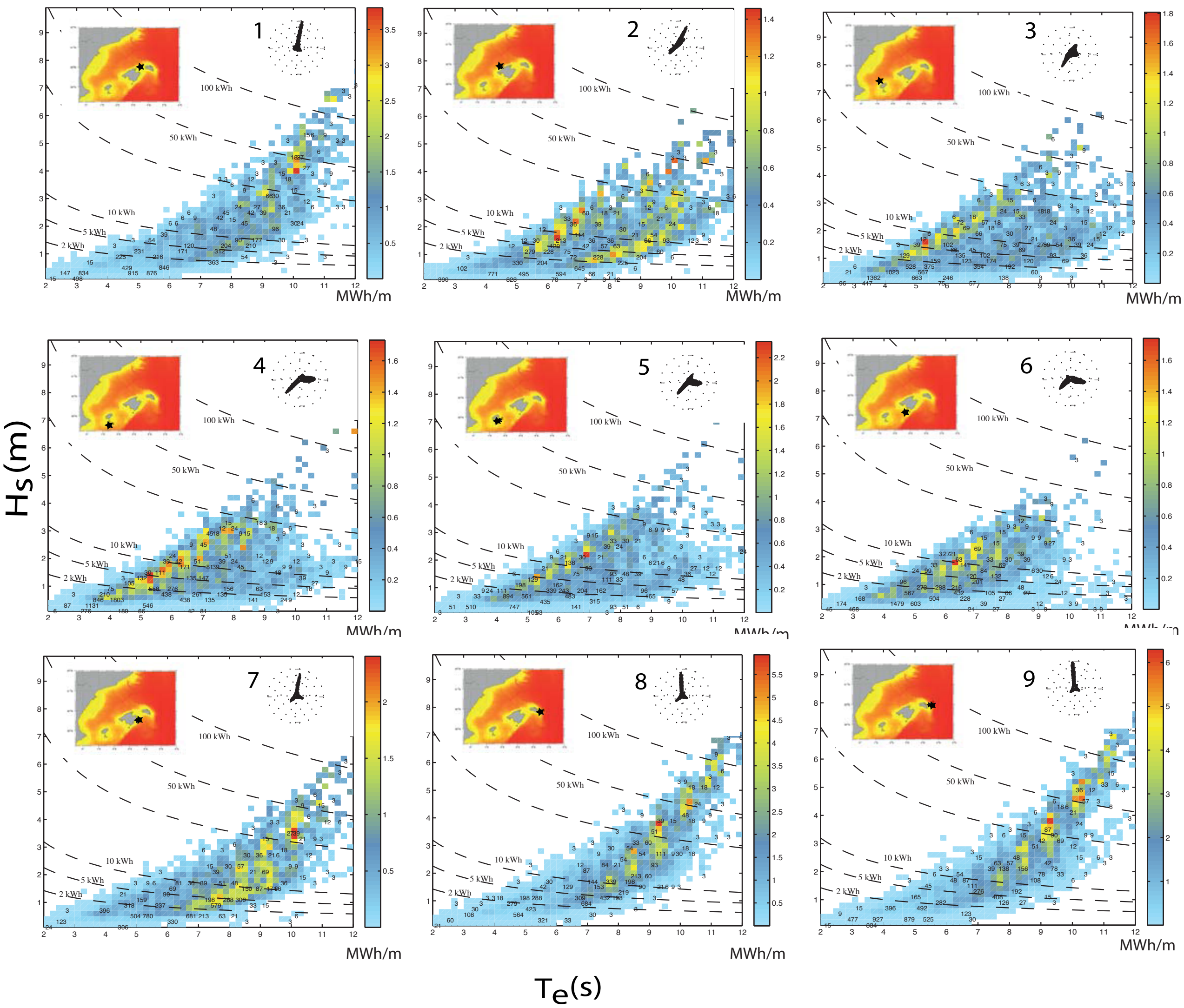

Figure 8: Contribution to the total annual energy for the different sea states at the different points around the Balearic Islands. Wave rose at each virtual node is depicted at the upper right side of each panel. Colors in MWh/m. The dashed lines correspond to contour lines of constant wave power.

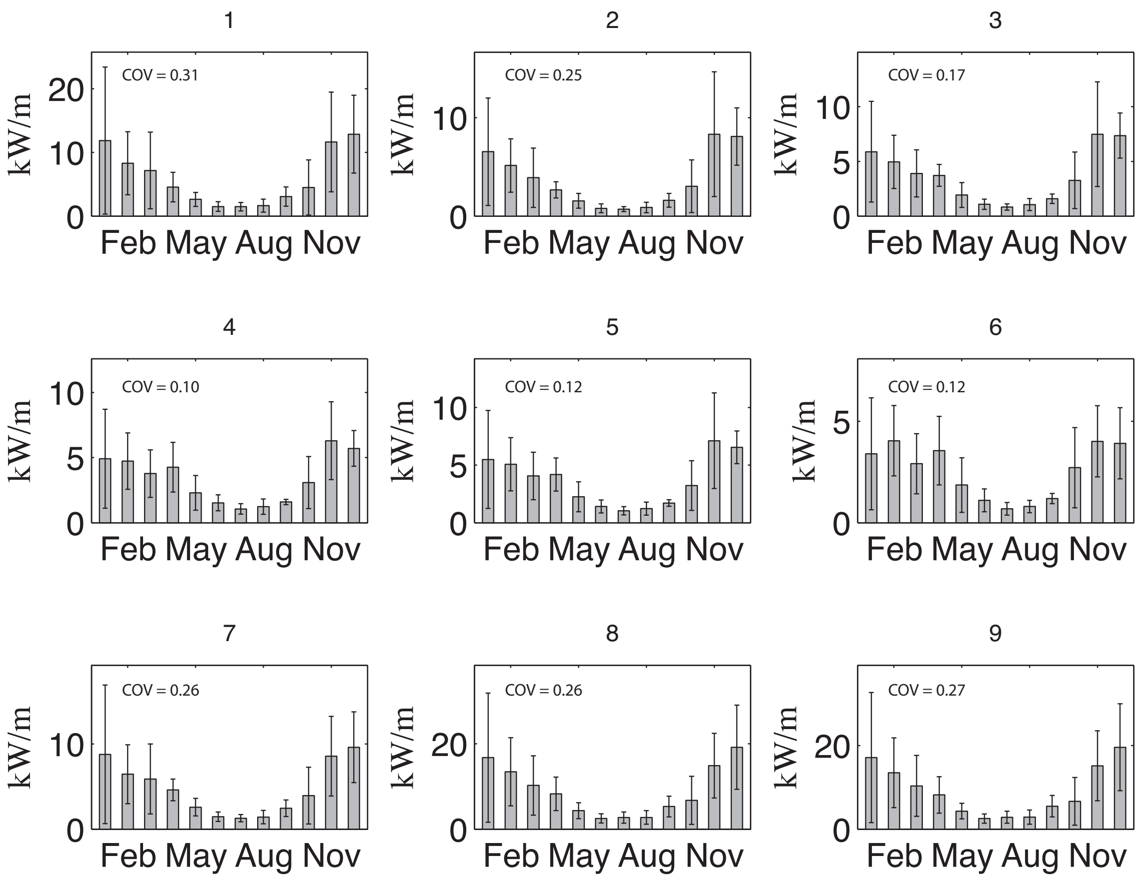

Figure 9: Average monthly energy flux with standard deviation for the selected points around the Balearic Archipelago.

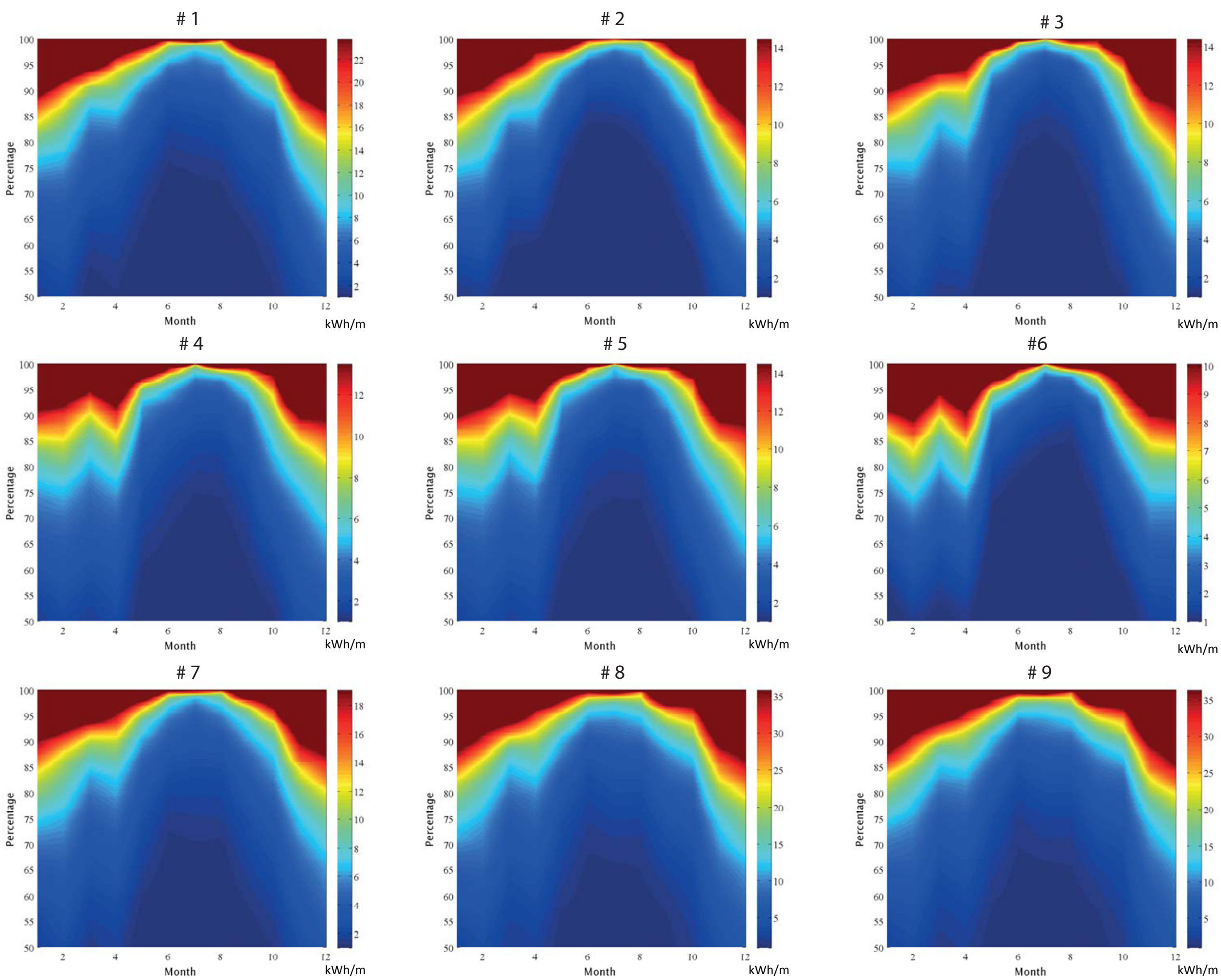

Figure 10: Percentage of non-exceedance of monthly energy flux provided by all sea states with standard deviation for the selected points around the Balearic Archipelago.